Bearing Fault Detection on Wind Turbine Gearbox Vibrations Using Generalized Likelihood Ratio-Based Indicators

Preprint

Kayacan Kestel,[1] Cédric Peeters,[1] Jérôme Antoni,[2] Shawn Sheng,[3] and Jan Helsen[1]

1 Vrije Universiteit Brussel
2 University of Lyon, INSA Lyon
3 National Renewable Energy Laboratory

Presented at ASME Turbo Expo 2022
Rotterdam, The Netherlands
June 13–17, 2022

NREL is a national laboratory of the U.S. Department of Energy
Office of Energy Efficiency & Renewable Energy
Operated by the Alliance for Sustainable Energy, LLC

This report is available at no cost from the National Renewable Energy Laboratory (NREL) at www.nrel.gov/publications.

Contract No. DE-AC36-08GO28308

Conference Paper
NREL/CP-5000-81777
August 2022

Bearing Fault Detection on Wind Turbine Gearbox Vibrations Using Generalized Likelihood Ratio-Based Indicators

Preprint

Kayacan Kestel,[1] Cédric Peeters,[1] Jérôme Antoni,[2] Shawn Sheng,[3] and Jan Helsen[1]

1 Vrije Universiteit Brussel
2 University of Lyon, INSA Lyon
3 National Renewable Energy Laboratory

Suggested Citation
Kestel, Kayacan, Cedric Peeters, Jerome Antoni, Shawn Sheng, and Jan Helsen. 2022. *Bearing Fault Detection on Wind Turbine Gearbox Vibrations Using Generalized Likelihood Ratio-Based Indicators: Preprint*. Golden, CO: National Renewable Energy Laboratory. NREL/CP-5000-81777. https://www.nrel.gov/docs/fy22osti/81777.pdf.

Conference Paper
NREL/CP-5000-81777
August 2022

National Renewable Energy Laboratory
15013 Denver West Parkway
Golden, CO 80401
303-275-3000 • www.nrel.gov

NOTICE

This work was authored in part by the National Renewable Energy Laboratory, operated by Alliance for Sustainable Energy, LLC, for the U.S. Department of Energy (DOE) under Contract No. DE-AC36-08GO28308. Funding provided by U.S. Department of Energy Office of Energy Efficiency and Renewable Energy Wind Energy Technologies Office. The views expressed herein do not necessarily represent the views of the DOE or the U.S. Government. The U.S. Government retains and the publisher, by accepting the article for publication, acknowledges that the U.S. Government retains a nonexclusive, paid-up, irrevocable, worldwide license to publish or reproduce the published form of this work, or allow others to do so, for U.S. Government purposes.

Cover Photos by Dennis Schroeder: (clockwise, left to right) NREL 51934, NREL 45897, NREL 42160, NREL 45891, NREL 48097, NREL 46526.

BEARING FAULT DETECTION ON WIND TURBINE GEARBOX VIBRATIONS USING GENERALIZED LIKELIHOOD RATIO-BASED INDICATORS

Kayacan Kestel[1], Cédric Peeters[1], Jérôme Antoni[2], Shawn Sheng[3], Jan Helsen[1]

[1]Vrije Universiteit Brussel, Brussels, Belgium
[2]Univ Lyon, INSA Lyon, Villeurbanne, France
[3]National Renewable Energy Laboratory, Golden, CO

ABSTRACT

Studies in condition monitoring literature often aim to detect rolling element bearing faults because they have one of the biggest shares among defects in turbo machinery. Accordingly, several prognosis and diagnosis methods have been devised to identify fault signatures from vibration signals. A recently proposed method to capture the rolling element bearing degradation provides the groundwork for new indicator families utilizing the generalized likelihood ratio test. This novel approach exploits the cyclostationarity and the impulsiveness of vibration signals independently in order to estimate the most suitable indicators for a given fault. However, the method has yet to be tested on complex experimental vibration signals such as those of a wind turbine gearbox. In this study, the approach is applied to the National Renewable Energy Laboratory Wind Turbine Gearbox Condition Monitoring Round Robin Study data set for bearing fault detection purposes. The data set is measured on an experimental test rig of a wind turbine gearbox; hence the complexity of the vibration signals is similar to a real case. The outcome demonstrates that the proposed method is capable of distinguishing between healthy and damaged vibration signals measured on a complex wind turbine gearbox.

Keywords: fault detection, likelihood ratio test, cyclostationary, impulsiveness, condition monitoring

NOMENCLATURE

BPFI	Ball pass frequency inner-race
BPFO	Ball pass frequency outer-race
CI	Condition indicators
GCS	Gaussian cyclostationary
GS	Gaussian stationary
GGS	Generalized Gaussian stationary
GGCS	Generalized Gaussian cyclostationary
GLR	Generalized likelihood ratio
MLE	Maximum-likelihood estimate
NREL	National Renewable Energy Laboratory
O&M	Operations and maintenance
PDF	Probability density function
SES	Squared envelope spectrum
TSA	Time-synchronous averaging

1. INTRODUCTION

The ever-increasing pursuit to use wind energy to cover a substantial portion of the energy demand comes paired with high operations and maintenance (O&M) costs. Hence, health monitoring of wind turbines has become a key point to minimize the O&M costs, particularly for offshore wind turbines, as their hard-to-access nature can amount to significant repair costs [1]. It is reported that O&M costs can be considerably reduced via well-scheduled maintenance planning [2], which necessitates efficient and continuous health monitoring of these complex devices. Accordingly, various techniques have been developed and used to assess the current state and the remaining lifetime of the wind turbine components, examples of which include oil, acoustic, and vibration analysis [3]. Particularly, vibration-based health monitoring appears to be a versatile tool, as it offers solutions for diagnosis and prognosis purposes for both the wind turbine structure and its rotating components. [4, 5]. Furthermore, considering the moving elements of the wind turbines such as the gearbox or the blades, bearing faults are the leading cause of machine failures; hence, numerous methods have been proposed in literature to better capture the bearing-related machine anomalies [6].

The present study aims to test the performance and applicability of a novel generalized likelihood ratio (GLR)-based method, which is devised as a groundwork for designing new condition indicators (CI) [7] for vibration-based health monitoring of rotating machinery. Given that bearing faults are the most frequently observed machine anomaly, the motivation is to detect bearing faults using the new CIs from vibration signals made available by the National Renewable Energy Laboratory (NREL) and collected from a full-scale wind turbine testing gearbox [8].

In general, indicators devised for vibration-based condition monitoring exploit two different signal properties that can be related to faults of components of rotating machinery. The first one is the prevalent presence of impulses in the vibration signal, which leads the distribution of a signal to deviate from Gaussianity. Probably, the most-used condition indicator to quantify the impulsiveness of a signal is kurtosis. The definition of kurtosis is that the fourth-order central moment of the signal distribution [9] and its deviation from Gaussianity can be interpreted as the presence of incipient or progressed bearing faults [7]. Other measures, similar to kurtosis, with higher-order moments have also been developed for condition monitoring purposes [10], yet they are not commonly used since they do not demonstrate robust fault indication with highly impulsive signals [7]. The second interesting property of vibration signals that can be utilized for condition monitoring purposes is the shift from statistical stationarity to non-stationarity. Particularly for the rolling element bearing faults, non-stationarity appears in the form of second-order cyclostationarity [11]. Methods that track cyclostationary signatures embedded in vibration signals are typically based on the squared envelope spectrum (SES). An example of such a method is a recent study that demonstrates a link between the sum of amplitudes of the SES with the kurtosis of the signal [12]. Measuring the sparsity of the SES is also introduced as a viable option to diagnose bearing faults by blind filtering the vibration signals [13]. Likewise, another study proposed an indicator of second-order cyclostationarity that is maximized through a blind deconvolution filter [14].

Antoni and Borghesani proposed a novel GLR-based method that leads to a new way of designing condition indicators by exploiting the two main properties of the vibration signal, which can be linked to a rolling element bearing fault [7]. Accordingly, several CIs are introduced. In the present study, the performance of these new indicators is tested. The underlying theory behind the design of the CIs is introduced in Section 2, as are the features of the NREL data set. In Section 3, the key findings of the study are demonstrated and discussed by elaborating on the reasoning behind the efficacy of the GLR-based indicators. The conclusive remarks are given in Section 4.

2. METHODOLOGY

This section provides a high-level overview of the underlying theory of the proposed indicators. Interested readers can refer to [7] for the full derivations.

One of the strong aspects of the proposed methodology is its intention to be optimal for testing the non-stationarity and non-Gaussianity of the vibration signal. In order to do so, a statistical tool called the likelihood ratio test is employed to assess the likelihood of the property of interest present in the signal.

2.1 Generalized Likelihood Ratio Test

The generalized likelihood ratio test requires two hypotheses to be tested. In essence, assumptions that a property is embedded in a signal and that the signal does not contain this property make two hypotheses. Respectively, the two hypothesis can be called H_1 and H_0 (null hypothesis). These hypotheses must be associated with the measured vibration signals in order to reveal whether or not the property of interest is present. Thus, different probability density functions (PDF) are defined such that the PDF parameters are estimated from the measured signals. The following expressions show the definitions of the probability functions:

$$\begin{aligned} H_0 &: x(n) \sim p_x(\boldsymbol{x}|H_0, \boldsymbol{\theta_0}) \\ H_1 &: x(n) \sim p_x(\boldsymbol{x}|H_1, \boldsymbol{\theta_1}) \end{aligned} \tag{1}$$

where p_x signifies the PDF, of which the parameters are represented by $\boldsymbol{\theta_0}$ or $\boldsymbol{\theta_1}$. Both $\boldsymbol{\theta}$ and $\boldsymbol{x}$ are represented with bold characters to indicate that they are either vector or matrix quantities, and the amplitude of a signal at any time n is noted with $x(n)$.

The GLR test is selected to be the most favourable approach to test which PDF represents the measured signal $\boldsymbol{x}$ among other candidates [7]. Examples may include the Wald test or Lagrange multiplier test [15]. The GLR test is defined as:

$$\Lambda(\boldsymbol{x}) = \frac{p_x(\boldsymbol{x}|H_1, \hat{\boldsymbol{\theta}}_{\boldsymbol{1}})}{p_x(\boldsymbol{x}|H_0, \hat{\boldsymbol{\theta}}_{\boldsymbol{0}})} \tag{2}$$

The quantities $\hat{\boldsymbol{\theta}}_{\boldsymbol{0}}$ and $\hat{\boldsymbol{\theta}}_{\boldsymbol{1}}$ are the maximum likelihood estimates (MLE) of the parameters space of the defined probability density functions, which link the measured signal with the proposed hypothesis. As the value of $\Lambda(\boldsymbol{x})$ increases, the test becomes more inclined to reject H_0. On the other hand, $\Lambda(\boldsymbol{x})$ tends to unity for the cases where H_0 holds. The GLR can also be expressed as a logarithm to ease the mathematical derivations in the likelihood function estimations. For its natural-log representation, $ln\Lambda(\boldsymbol{x})$ tends to zero for the cases where the null hypothesis, H_0, holds, as expected.

2.2 Indicator Design and Employed Indicators

The proposed methodology states that any indicator, using the concept of the log-generalized likelihood ratio, can be defined as:

$$ln\Lambda(\boldsymbol{x}) = \sum_{n=0}^{L-1} lnp_x(\boldsymbol{x}|H_1, \hat{\boldsymbol{\theta}}_{\boldsymbol{1}}) - \sum_{n=0}^{L-1} lnp_x(\boldsymbol{x}|H_0, \hat{\boldsymbol{\theta}}_{\boldsymbol{0}}) \tag{3}$$

Hence, with $\mathcal{L}_{H_1}$ and $\mathcal{L}_{H_0}$ being the log-likelihoods of hypotheses H_1 and H_0, Eq. 3 can be rewritten as:

$$I_{H_1/H_0} = c\frac{\mathcal{L}_{H_1} - \mathcal{L}_{H_0}}{L} \geq 0 \tag{4}$$

Note that the division by L, the signal length, is to ensure that the indicator is asymptotically constant, and c is a calibration parameter that just simplifies the final expression. Employing the definition of the indicator shown in Eq. 4, three different indicators are briefly explained and their performances are tested on experimental signals. Three indicators are compared:

- Cyclostationarity under Gaussian hypothesis
- Cyclostationarity under non-Gaussian hypothesis
- Non-Gaussianity under stationary hypothesis

Cyclostationarity under Gaussian hypothesis.

This first indicator tests the null hypothesis, H_0, against the alternative hypothesis, under the assumption that the signal is distributed according to a Gaussian law. The hypotheses compared are as follows:

$$\begin{aligned} H_0 &: x \sim \mathcal{N}(\boldsymbol{x}; 0, \sigma^2) \\ H_1 &: x \sim \mathcal{N}(\boldsymbol{x}; 0, \boldsymbol{\sigma}^2(n)) \end{aligned} \tag{5}$$

where $\boldsymbol{\sigma}^2(n)$ is the N-periodic variance. The hypotheses defined in Eq. 5 are following a Gaussian distribution with zero mean, which refers to the removal of the deterministic part of the signal. The final version of the indicator, $I_{GCS/GS}$, which tests Gaussian cyclostationarity versus Gaussian stationarity, can be written as:

$$I_{GCS/GS}(\boldsymbol{x}) = ln\langle s^2(n)\rangle - \langle ln(s^2(n))\rangle \tag{6}$$

and the quantity $s^2(n)$, which stands for the N-periodic component of the squared envelope of the signal, is estimated as follows:

$$s^2(n) = \frac{1}{K}\sum_{k=0}^{K-1} |x(n+kN)|^2 \tag{7}$$

where N is the number of points in the period of the interested cyclostationary signature, and the number of cycles in the signal designated with K can be estimated as $K = L/N$.

Cyclostationarity under non-Gaussian hypothesis.

The stationarity of the signal is tested under the assumption that the signal is distributed according to the generalized Gaussian distribution. Hence, the null and the test hypotheses are defined using a generalized Gaussian PDF as follows:

$$\begin{aligned} H_0 &: x \sim G\mathcal{N}(\boldsymbol{x}; 0, \eta, \beta) \\ H_1 &: x \sim G\mathcal{N}(\boldsymbol{x}; 0, \boldsymbol{\eta}(n), \beta) \end{aligned} \tag{8}$$

The quantity η is a scale parameter, analogous to the variance or periodic variance for $\eta(n)$, and β is the shape factor. Given the PDF of the hypotheses, the final version of the indicator, $I_{GGCS/GGS}$, which tests non-Gaussian cyclostationarity versus non-Gaussian stationarity, can be expressed as:

$$I_{GGCS/GGS}(\boldsymbol{x}) = 2\hat{\beta}_0^{-1} ln\langle s^{\hat{\beta}_0}(n)\rangle - 2\hat{\beta}_1^{-1}\langle lns^{\hat{\beta}_1}(n)\rangle + 2C \tag{9}$$

and the explicit version of C is as follows:

$$C(c, \hat{\beta}_0, \hat{\beta}_1) = ln\left(\frac{\hat{\beta}_0^{\frac{1}{\hat{\beta}_0}-1}\Gamma(c/\hat{\beta}_0)}{\hat{\beta}_1^{\frac{1}{\hat{\beta}_1}-1}\Gamma(c/\hat{\beta}_1)}\right) + \frac{1}{\hat{\beta}_0} - \frac{1}{\hat{\beta}_1} \tag{10}$$

where the lower case c is equal to 1 for real valued signals, and $\hat{\beta}_1$ and $\hat{\beta}_0$ correspond to the MLE of the shape parameters of the PDF of H_1 and H_0, respectively. For the generalized Gaussian family, the envelope of the N-periodic component is expressed with β rather than its square. Then, in Eq. 7 the squared envelope $s^2(n)$ is modified as $s^{\beta}(n)$.

Non-Gaussianity under stationary hypothesis.

The last indicator employed in this study tests the generalized Gaussian hypothesis against the Gaussian hypothesis under the stationary assumption. Proceeding from the following hypotheses definitions:

$$\begin{aligned} H_0 &: x \sim \mathcal{N}(\boldsymbol{x}; 0, \sigma) \\ H_1 &: x \sim G\mathcal{N}(\boldsymbol{x}; 0, \boldsymbol{\eta}, \beta) \end{aligned} \tag{11}$$

the indicator, $I_{GGS/GS}$, which tests non-Gaussian stationarity versus Gaussian stationarity, can be defined as:

$$I_{GGS/GS}(\boldsymbol{x}) = ln\langle|x(n)|^2\rangle - \frac{2}{\hat{\beta}} ln\langle|x(n)|^{\hat{\beta}}\rangle + 2C(c, 2, \hat{\beta}) \tag{12}$$

The function C is as expressed in Eq. 10 and $\hat{\beta}$ is again the MLE of the shape parameter of the generalized Gaussian PDF.

Three indicators defined in Eqs. 6, 9, and 12 are chosen to be tested in this study due to their superior performances as reported in the original study [7].

2.2.1 Use of a non-integer cyclic period.

One of the crucial parameters that is required for the efficient utilization of the proposed theory is the cyclic period (or the cyclic frequency) of the phenomenon of interest. Given that the motivation of the study is the detection of rolling bearing faults, the exact cyclic frequency often is an unknown because of the stochastic nature of rolling element bearings. By definition, the quantity N introduced in Eq. 7 is directly associated with the cyclic period. Hence, it poses a problem when N is not an integer because N, by definition, must be an integer. The latter problem can be addressed either by using a zeroth-order interpolation for the estimation of $s^2(n)$ or by truncating the signal to a length at which N is an integer. A solution to the former problem is to accept a cyclic period [7], hence N, as another parameter to be considered in the MLE. Thus, an outer search grid is employed to perform the MLE for each value of N within the limits around the theoretical cyclic period. Therefore, Eq. 2 becomes:

$$\Lambda(\boldsymbol{x}) = \max_{N_{min} \le N \le N_{max}} \frac{p_x(\boldsymbol{x}|H_1, \hat{\boldsymbol{\theta}}_{\mathbf{1}}^{(N)})}{p_x(\boldsymbol{x}|H_0, \hat{\boldsymbol{\theta}}_{\mathbf{0}})} \tag{13}$$

In the present study, for the non-integer values of N, zeroth-order interpolation is used.

2.3 Description of the Data Set

The performance of the new indicators is tested using the benchmarking data set of wind turbine gearbox vibration signals made available by NREL [8]. The full-scale experimental wind turbine gearbox setup is designed to be stall-controlled and three-bladed and to have a rated power of 750 kW. A representation of the test turbine provided in the NREL report can be seen in Fig. 1. The experimental vibration signals are collected from two gearboxes with an identical design which are in "Healthy" and "Damaged" conditions. The vibration signals investigated in this study are recorded at the average rotational speed of the high-speed shaft (HSS) of 1,800 rpm from twelve different accelerometers; the speed measurements of the HSS are also made available via an optical encoder. The signals are sampled at

40, 000 Hz for 60 seconds and 10 measurements are recorded for each "Healthy" and "Damaged" state of the gearbox.

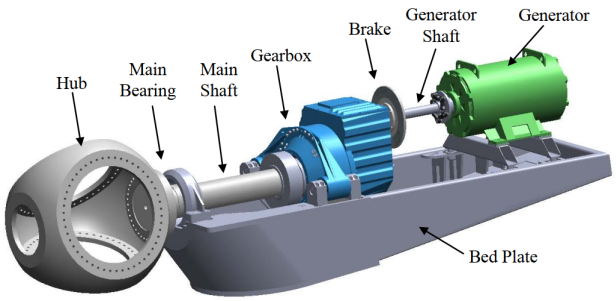

FIGURE 1: REPRESENTATION OF THE NREL WIND TURBINE GEARBOX TEST SETUP [8]

The gearbox includes numerous bearings and their types are reported in the NREL study [8]. According to the report, seven different damage types that gearbox contains can be detectable with vibration analysis. Among the reported damages, three cases that are also investigated in other studies [16, 17] are chosen to be the candidates for the test of the limits of the novel indicator design. These are the fault signatures contained in the signals measured from the accelerometers AN5, AN6, and AN7. Accordingly, the full-complement cylindrical roller bearing (fcCRB) and two tapered roller bearings (TRB) are the source of the fault signatures [8]. In Table 1, a summary of the bearing characteristics, which includes characteristic frequency, root cause of the bearing fault, and the label of the accelerometer in the vicinity of the related faulty bearing, is provided. The types of the bearing faults, namely the ball pass frequency inner-race (BPFI), the fundamental train frequency (FTF), and the ball pass frequency outer-race (BPFO), are also listed in Table 1.

3. RESULTS AND DISCUSSION

The first step of the vibration signal process is angular resampling. The NREL data set already includes the instantaneous angular speed (IAS) measurements; hence, angular resampling is performed to compensate for the speed variations. Now that the high-energy peaks in the frequency spectrum are more pronounced, the indicators can be estimated.

3.1 Signals from AN7

Because it is reported that the fault signature of the BPFI in signals from sensor AN7 is the most prominent [16], vibration signals from this sensor are processed first . The zoomed envelope around the BPFI of 345.3 Hz is demonstrated for healthy and damaged signals in Fig. 2. The strong peak around 345 Hz is already an indication of a bearing fault.

As can be seen in Eqs. 5, 8, and 11, the proposed method is based on associating the signal distribution with a possible rolling element bearing fault. Hence, the signal must be prewhitened in order to ensure the deterministic content of the signal does not skew its distribution. It may be misleading if the signal deviates from Gaussianity due to the deterministic content. Thus, in this study, cepstral editing is chosen to be the prewhitening method.

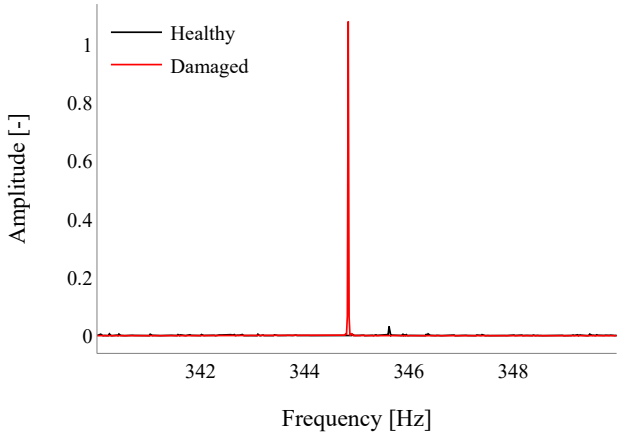

FIGURE 2: ZOOMED ENVELOPE SPECTRUM OF A HEALTHY AND A DAMAGED SIGNAL MEASURED FROM SENSOR AN7

Because the average rotational speed of the HSS is 30Hz, a long-pass lifter with quefrency cutoff of $1/50 = 0.02$ s is applied to the signals.

Ensuring that the deterministic content is removed from the signals, the indicator test can be carried out. Two indicators introduced in Eqs. 5 and 8 require a good estimation of the value N; hence, as mentioned, an outer search algorithm is employed for the MLE of the parameters of $I_{GCS/GS}$ and $I_{GGCS/GGS}$. Because the expected slippage for a rolling element bearing is a few percent of the theoretical characteristic frequency [18], the limits of the outer search range of N are also chosen accordingly. Assuming the slippage is no more than ±2%, the lower and the upper limits of the N search range are calculated as follows:

$$\begin{aligned} N_{lower} &= F_s/(f_{BPFI} + f_{BPFI} \times 0.02) \\ N_{upper} &= F_s/(f_{BPFI} - f_{BPFI} \times 0.02) \end{aligned} \tag{14}$$

where f_{BPFI} corresponds to the theoretical frequency of the BPFI and F_s is the sampling frequency. While $I_{GCS/GS}$ and $I_{GGCS/GGS}$ require the BPFI frequency estimation, $I_{GGS/GS}$ does not.

Throughout the study, standard box plots are used to show the levels of the indicators. Because the data set comprises 10 measurements of the healthy and damaged signals, an increasing trend with the indicators, which may imply continuous degradation of a bearing fault, is not expected. Rather, a step increase between the indicator levels of the healthy and damaged states of the gearbox is anticipated. Hence, the indicator estimations for each measurement are clustered into two boxes, which represent the two different states of the machine.

For the indicators that track the cyclostationary behaviour in the signals measured from AN7, the difference between the medians of the indicators of the healthy and the damaged signals in Fig. 3 is insignificant. Moreover, while the $I_{GCS/GS}$ and the $I_{GGCS/GGS}$ of the healthy signals have very low variance, those of damaged signals have high variance, with a single outlier for each. This may indicate that the MLE of the parameters is not optimal with regards to the prediction of the state of the signal.

Bearing type	Mode	Sensor label	Fault type	Characteristic frequency
TRB	Overheating	AN7	BPFI	345.3 Hz
TRB	Overheating	AN7	FTF	12.8 Hz
TRB	Assembly damage, dents	AN6	BPFO	105.3 Hz
TRB	Assembly damage, dents	AN6	BPFI	73.7 Hz
fcCRB	Fretting corrosion	AN5	BPFO	8.8 Hz

TABLE 1: SUMMARY OF THE BEARING FAULTS

On the other hand, the increase in the median of $I_{GGS/GS}$ of the damaged signals to that of the healthy ones is around 35 times. While the significant increase in $I_{GGS/GS}$ can be considered as an indication of the bearing fault, it may not be directly related to the BPFI. As listed in Table 1, signals of sensor AN7 contain two different bearing faults; hence, the presence of abundant impulses is very likely. Therefore, what $I_{GGS/GS}$ indicates may be the effect of the combination of the two faults. Nonetheless, despite only requiring prewhitening, $I_{GGS/GS}$ performed well to indicate an anomaly that causes impulses in the signals.

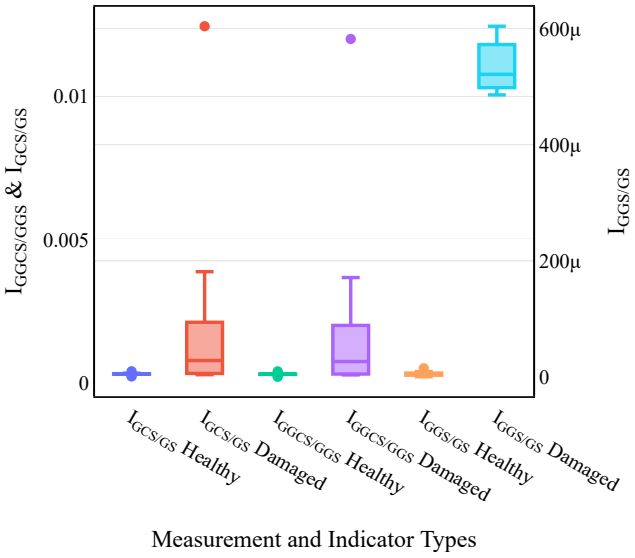

FIGURE 3: BOX PLOT REPRESENTATION OF $I_{GCS/GS}$, $I_{GGCS/GGS}$, AND $I_{GGS/GS}$ FOR HEALTHY AND DAMAGED SIGNALS MEASURED FROM SENSOR AN7

Given the weak performances of $I_{GCS/GS}$ and $I_{GGCS/GGS}$, the underlying theory in the design of the indicators based on non-stationarity is further scrutinized. Eq. 5 is merely the function of $s^2(n)$, which is the time-synchronous averaged squared envelope. Time-synchronous averaging (TSA) is a strong tool in vibration-based health monitoring, particularly for phenomena that are purely cyclostationary, such as a gear tooth fault. As a consequence of the slippage phenomenon, the faulty signature of rolling element bearing faults is accepted to be quasi-cyclostationary. In other words, the phase of the cyclostationary behaviour from a rolling element bearing fault may slightly shift over time. Therefore, as a signal lasts longer, the performance of TSA deteriorates more. Given that, estimating $s^2(n)$ for a 60-second signal that has 2.4 million points may be problematic. Therefore, using only the first 1, 2, 5, 10, 20 seconds, and the entire damaged signal, the quantity $s^2(n)$ is estimated. The first 450 points of $s^2(n)$ calculated for the five different signal lengths are shown in Fig. 4. For the BPFI of 345.3 Hz, the corresponding approximate N values are 115; Fig. 4 is thus expected to contain 4 cycles. While 4 cycles are clearly observable over $s^2(n)$ of the signals of 1, 2, 5, and 10 seconds, the 20-second signal and the entire signal seem to lose the impulsive pattern. Hence, using a truncated form of a signal appears to be an efficient way of estimating $s^2(n)$.

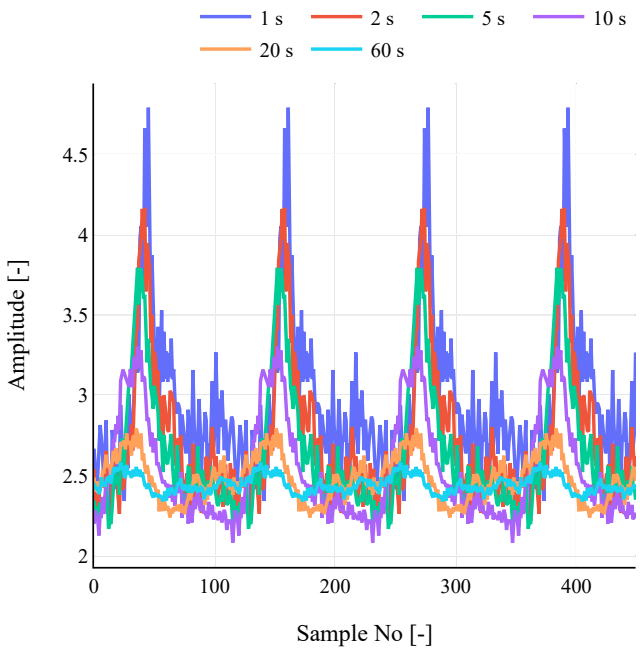

FIGURE 4: TIME-SYNCHRONOUS AVERAGED SQUARED ENVELOPE - $s^2(n)$

The cyclostationarity-based indicators can be estimated using shorter signals. According to Fig. 4, the $s^2(n)$ of a 1-second signal demonstrates the peaks with the highest amplitudes. In other words, the signal-to-noise ratio (SNR) of the time-synchronous averaged squared envelope is the highest. Therefore, each measurement of the sensor AN7 is divided into 1-second signals. Thus, 600 sub-signals are generated for each of the healthy and damaged states of the gearbox over which the $I_{GCS/GS}$ and the $I_{GGCS/GGS}$ are calculated, and the findings are displayed in Fig. 5. A clear increase in the medians of the indicators corresponding to the damaged signals is noticeable compared to the

ones in Fig. 3. Hence, now the difference between the indicators' levels of the healthy and the damaged signals is more prominent. This also confirms that shortening the signal in order to improve the TSA also increases the likelihood of the detection of a possible rolling element bearing fault. On the other hand, for the lower theoretical fault frequencies, a 1-second signal is not enough to properly estimate the $s^2(n)$ such that the SNR is high enough, because the approximate value of N remains large compared to the length of a second signal. Furthermore, the shortening of the signal length also reduces the frequency resolution, which is not desirable. Therefore, there must be an optimal signal length at which the $s^2(n)$ demonstrates the most pronounced cyclostationary behaviour.

It may be important to mention that the outliers in Fig. 3 are approximately equal to the medians in Fig. 5 for the same indicators of the damaged signals. This may imply that in 1 out of 10 measurements, the slippage is not strong, and therefore the $s^2(n)$ estimation is not affected significantly. One interesting point with regards to the results in Fig. 5 is that the variance and the median of both $I_{GCS/GS}$ and $I_{GGCS/GGS}$ of healthy signals also increased, which indicates that the signature of the BPFI was already present, even in the healthy data.

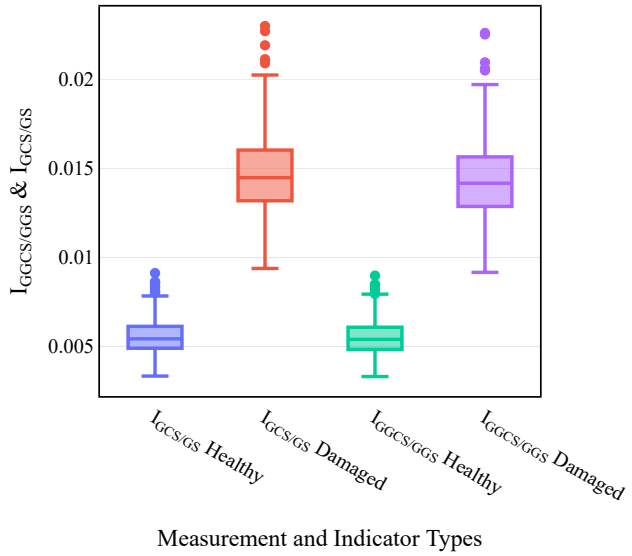

FIGURE 5: BOX PLOT REPRESENTATION OF $I_{GCS/GS}$ AND $I_{GGCS/GGS}$ FOR 1-SECOND LENGTH OF HEALTHY AND DAMAGED SIGNALS MEASURED FROM SENSOR AN7

3.2 Signals from AN5 & AN6

The indicators are also tested with the signals measured from sensors AN5 and AN6. The zoomed envelope spectra of AN5 and AN6 are shown in Figs. 6 and 7, respectively. The signature of the BPFO appears to be buried in the noise floor of the envelope spectrum of AN5. The two peaks purported in Fig. 6 are the first and the second harmonics of 7.50 Hz, which is the frequency of the rotational speed of the intermediate-speed shaft (IMS). The BPFO of the damaged signal from AN6, on the other hand, is slightly more visible compared to that of AN5. The black marker represents the position of the BPFO of 105.3 Hz in Fig. 7.

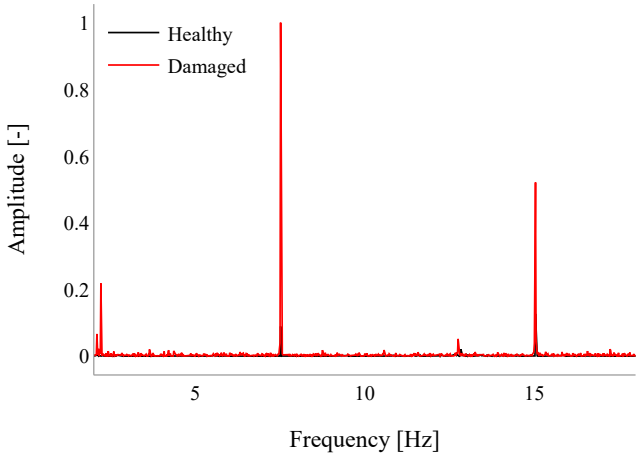

FIGURE 6: ZOOMED ENVELOPE SPECTRUM OF THE SIGNAL MEASURED FROM SENSOR AN5

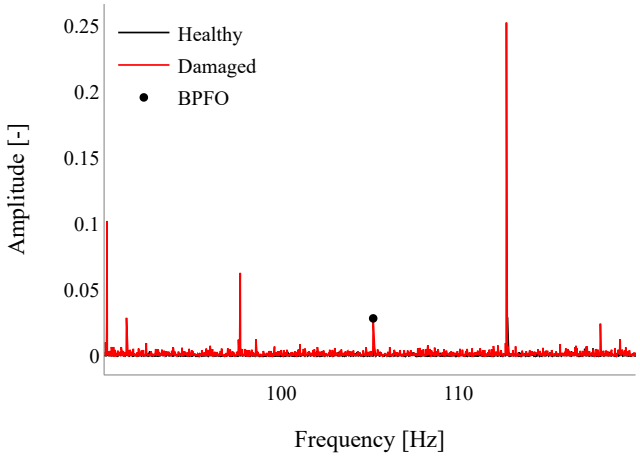

FIGURE 7: ZOOMED ENVELOPE SPECTRUM OF THE SIGNAL MEASURED FROM SENSOR AN6

Given that the fault frequency is hidden for AN5 and weak for AN6, the indicator based on impulsiveness of the signals is tested first and the results are shown in Fig. 8. A clear elevation of the medians of the $I_{GGS/GS}$ is visible for both signals from AN5 and AN6, which can be associated with a rolling element bearing fault. Such increase in the $I_{GGS/GS}$ can also be related to the other sources of vibration generating impulses because the $I_{GGS/GS}$ is based on impulsiveness of the signal. In other words, while the damaged signals are recorded, there are several other damages reported in the gearbox at various other locations. Therefore, the ones that are in the proximity of sensor AN5 and AN6 may result in impulses in these channels. Nevertheless, the indicator $I_{GGS/GS}$ drastically increased from the healthy state to the damaged state of the gearbox for both AN5 and AN6, which can be associated with the rolling element bearing fault. The cyclostationarity-based indicators, on the other hand, do not demonstrate any significant difference between the healthy and the damaged signals of AN5, and thus are not presented.

Measurements from AN6 are further tested for the

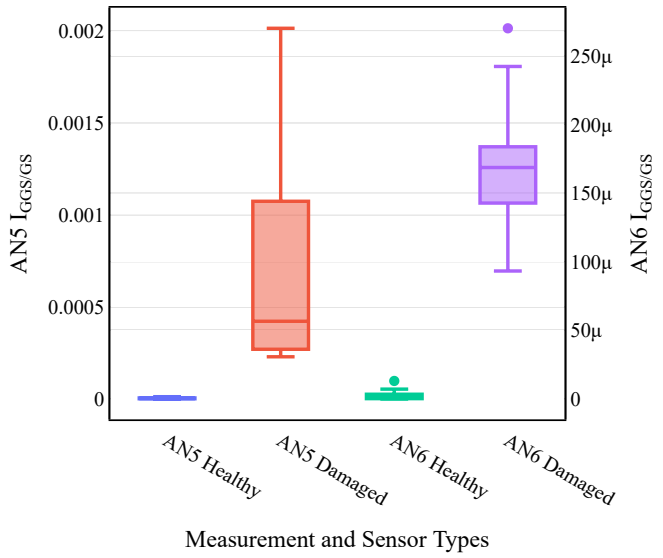

FIGURE 8: BOX PLOT REPRESENTATION OF $I_{GGS/GS}$ FOR THE SIGNALS MEASURED FROM AN5 AND AN6

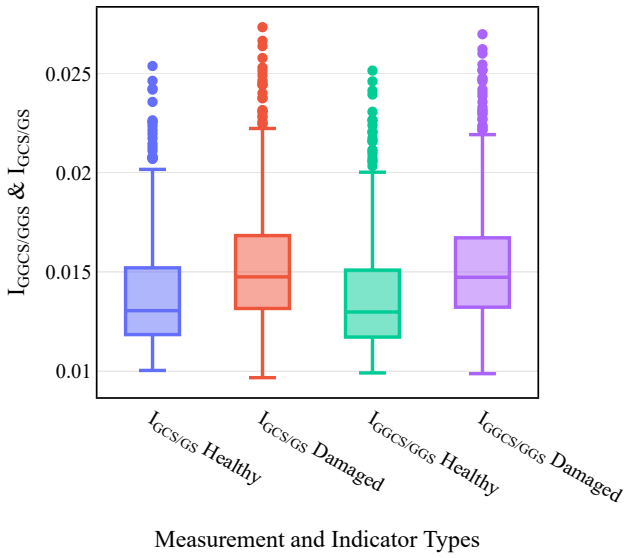

FIGURE 9: BOX PLOT REPRESENTATION OF $I_{GCS/GS}$ AND $I_{GGCS/GGS}$ INDICATORS ESTIMATED USING SIGNALS FROM AN6

cyclostationary-based indicators. As mentioned above, the measurements from AN6 are also divided into 1-second signals and both the $I_{GCS/GS}$ and the $I_{GGCS/GGS}$ are estimated. According to the results shown in Fig. 9, there is a slight increase around 15% between the medians of the indicator levels of the healthy and damaged states of the machine. Furthermore, indicators for both states of the gearbox spread over a wide range with several outliers. The reason behind this can be twofold. The first is that both the $I_{GCS/GS}$ and the $I_{GGCS/GGS}$ are not capable of detecting the bearing fault for the given severity of the fault with strong confidence. The second reason can be that the healthy data also contains the fault related to the cyclostationary signature; hence, the elevation of the medians of the indicators from the healthy to the damaged state is not clear-cut. The presence of multiple damages, including an assembly damage, is also reported in [8], thus the latter reasoning is more likely to be valid. However, this does not fully explain the absence of the BPFO for the healthy signal, while it appears weak in the damaged signal in Fig. 7.

In order to better comprehend the insight of the estimation of the $I_{GCS/GS}$ and the $I_{GGCS/GGS}$ on the signals of AN6, the spectrum of $s^2(n)$ is displayed in Fig. 10. The figure shows the first 10 harmonics of the BPFO for the healthy and the damaged $s^2(n)$ spectrum. From an alternative representation of Eq. 6 expressed as

$$I_{GCS/GS} = -\left\langle ln\left(\frac{s^2(n)}{\langle s^2(n)\rangle}\right)\right\rangle \tag{15}$$

the indicator can be interpreted as the ratio energy of the $s^2(n)$ and its mean. Considering Fig. 10, although the amplitudes of the harmonics of the BPFO for the damaged signal are higher than that for the healthy signal, the mean of $s^2(n)$ of the damaged signal is also almost 2 times the healthy one. Hence, the indicator levels for the healthy and the damaged signals are not significantly different. The means of $s^2(n)$ are so high that they dwarf the other amplitudes, thus the zeroth frequency bin is not shown in Fig. 10.

Similar discussions regarding $I_{GCS/GS}$, or $s^2(n)$, can also be made for $I_{GGCS/GGS}$, or $s^{\hat{\beta}}(n)$. However, because the $I_{GGCS/GGS}$ requires the estimation of the shape parameter β for each TSA envelope, the comparison is more complicated. Therefore, in order to keep the discussion brief, this part is not elaborated. Apart from that, since these two indicators simply test the cyclostationarity against the stationarity, their values are near each other for every signal. This also indicates the robustness of the proposed method.

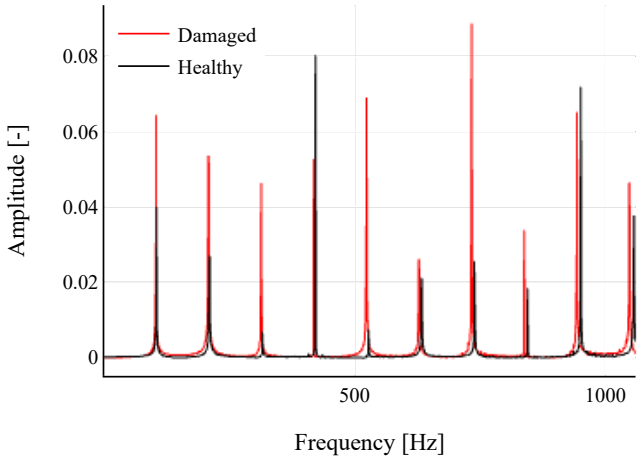

FIGURE 10: THE SPECTRUM OF TSA ENVELOPE OF A HEALTHY AND A DAMAGED SIGNAL MEASURED FROM AN6

The discussion about the signal length can be extended to devise a parameter to measure the optimal estimation of $s^2(n)$ and the signal length can be taken into account as a new parameter for MLE, like the quantity N. With regards to that, a way of assessing how well $s^2(n)$ represents the cyclostationarity related with the interested frequency must be investigated.

4. CONCLUSION

The proposed method that uses GLR in order to devise new CIs to detect rolling element bearing faults is tested on the complex vibration signals measured on an experimental test rig of a wind turbine gearbox. The conclusion of this study is threefold. Firstly, the new condition monitoring indicators are promising in terms of detecting rolling element bearing faults on experimental data. Secondly, due to the slippage phenomenon, tracking the cyclostationary signatures embedded in the signal via time-synchronous averaging-based indicators may be misleading for considerably long signals or for high slippage occurrences. Therefore, the signal length becomes another parameter to be taken into account in maximum likelihood estimations of the parameter space. Lastly, the time-synchronous averaged squared envelope may be further employed to form novel condition indicators. The last two remarks may pave the way for further research aiming to improve the GLR-based indicators.

ACKNOWLEDGMENTS

Jan Helsen received funding from the Flemish Government (AI Research Program). The authors would also like to acknowledge FWO (Fonds Wetenschappelijk Onderzoek) for their support through the post-doctoral grant of Cédric Peeters (#1282221N). They would also like to acknowledge FWO for the support through the SBO Robustify project (S006119N). The authors would also like to acknowledge the support of De Blauwe Cluster through the project Supersized 4.0 and the agency for Innovation by Science and Technology in Belgium for supporting the SIM MaSiWEC project.

This work was authored in part by the National Renewable Energy Laboratory, operated by Alliance for Sustainable Energy, LLC, for the U.S. Department of Energy (DOE) under Contract No. DE-AC36-08GO28308. Funding provided by the U.S. Department of Energy Office of Energy Efficiency and Renewable Energy Wind Energy Technologies Office. The views expressed in the article do not necessarily represent the views of the DOE or the U.S. Government. The U.S. Government retains and the publisher, by accepting the article for publication, acknowledges that the U.S. Government retains a nonexclusive, paid-up, irrevocable, worldwide license to publish or reproduce the published form of this work, or allow others to do so, for U.S. Government purposes.

REFERENCES

[1] Helsen, J. "Review of Research on Condition Monitoring for Improved O&M of Offshore Wind Turbine Drivetrains." *Acoustics Australia* Vol. 49 No. 2 (2021): pp. 251–258. DOI 10.1007/s40857-021-00237-2.

[2] Walford, C. "Wind turbine reliability: understanding and minimizing wind turbine operation and maintenance costs." DOI 10.2172/882048. URL https://doi.org/10.2172%2F882048.

[3] F. P. G. Márquez, J.M.P. Pérez M. Papaelias, A.M. Tobias. "Condition monitoring of wind turbines: Techniques and methods." *Renewable Energy* Vol. 46 (2012): pp. 169–178. DOI 10.1016/j.renene.2012.03.003.

[4] M. Martinez-Luengo, A. Kolios and Wang, L. "Structural health monitoring of offshore wind turbines: A review through the Statistical Pattern Recognition Paradigm." *Renewable and Sustainable Energy Reviews* Vol. 64 (2016): pp. 91–105. DOI 10.1016/j.rser.2016.05.085.

[5] Sheng, S. and Veers, P. "Wind Turbine Drivetrain Condition Monitoring - An Overview." Golden, CO: National Renewable Energy Laboratory. NREL/CP-5000-50698. (2011). URL https://www.osti.gov/biblio/1029027.

[6] R. B. Randall, J. Antoni. "Rolling element bearing diagnostics—A tutorial." *Mechanical Systems and Signal Processing* Vol. 25 No. 2 (2011): pp. 485–520. DOI 10.1016/j.ymssp.2010.07.017.

[7] J. Antoni, P. Borghesani. "A statistical methodology for the design of condition indicators." *Mechanical Systems and Signal Processing* Vol. 114 (2019): pp. 290–327. DOI 10.1016/j.ymssp.2018.05.012.

[8] Sheng, S. "Wind Turbine Gearbox Condition Monitoring Round Robin Study - Vibration Analysis." Technical Report No. NREL/TP-5000-54530. Golden, CO: National Renewable Energy Laboratory. 2012. DOI 10.2172/1048981.

[9] A.M. Fiori, M. Zenga. "Karl Pearson and the Origin of Kurtosis." *International Statistical Review* Vol. 77 No. 1 (2009): pp. 40–50. DOI 10.1111/j.1751-5823.2009.00076.x.

[10] M. Cocconcelli, R. Rubini, G. Curcurù. "Statistical evidence of central moment as fault indicators in ball bearing diagnostics." *Proceedings of the 9th International Conference on Surveillance*. Fes (Marocco), May 22-24, 2017.

[11] R.B. Randall, S. Chobsaard, J. Antoni. "The relationship between spectral correlation and envelope analysis in the diagnostic of bearing faults and other cyclostationary machine signals." *Mechanical Systems and Signal Processing* Vol. 15 No. 5 (2001): pp. 945–962. DOI 10.1006/mssp.2001.1415.

[12] P. Borghesani, S. Chatterton, P. Pennacchi. "The relationship between kurtosis- and envelope-based indexes for the diagnostic of rolling element bearings." *Mechanical Systems and Signal Processing* Vol. 43 (2014): pp. 25—43. DOI 10.1016/j.ymssp.2013.10.007.

[13] C. Peeters, J. Helsen, J. Antoni. "Blind filters based on envelope spectrum sparsity indicators for bearing and gear vibration-based condition monitoring." *Mechanical Systems and Signal Processing* Vol. 138 (2020): p. 106556. DOI 10.1016/j.ymssp.2019.106556.

[14] M. Buzzoni, G. D'Elia, J. Antoni. "Blind deconvolution based on cyclostationarity maximization and its application to fault identification." *Journal of Sound and Vibration* Vol. 432 (2018): pp. 569–601. DOI 10.1016/j.jsv.2018.06.055.

[15] Buse, A. "The Likelihood Ratio, Wald, and Lagrange Multiplier Tests: An Expository Note." *The American Statistician* Vol. 36 No. 3 (1982): p. 153. DOI 10.2307/2683166.

[16] C. Peeters, J. Helsen, P. Guillaume. "Vibration-based bearing fault detection for operations and maintenance cost reduction in wind energy." *Renewable Energy* Vol. 116 (2018): pp. 74–87. DOI 10.1016/j.renene.2017.01.056.

[17] A. Mauricio, K. Gryllias, J. Qi. "Vibration-Based Condition Monitoring of Wind Turbine Gearboxes Based on Cyclosta-

tionary Analysis." *Journal of Engineering for Gas Turbines and Power* Vol. 141 No. 3. DOI 10.1115/1.4041114.

[18] Antoni, J. and Randall, R.B. "Differential diagnosis of gear and bearing faults." *J. Vib. Acoust.* Vol. 124 No. 2 (2002): pp. 165–171. DOI 10.1115/1.1456906. URL https://doi.org/10.1115%2F1.1456906.